STRUCTURAL CONTROL AND HEALTH MONITORING
Struct. Control Health Monit. 2011; **18**:852–868
Published online 5 August 2010 in Wiley Online Library (wileyonlinelibrary.com). DOI: 10.1002/stc.406

Optimal static output feedback control of a building using an MR damper

Sharadkumar Purohit and Naresh K. Chandiramani*,†

Department of Civil Engineering, Indian Institute of Technology Bombay, Mumbai 400076, India

SUMMARY

Optimal static output feedback (OSOF) control is used to obtain the control force desired from a magnetorheological (MR) damper fitted between ground and first storey of a three-storey building model. The modified Bouc–Wen model is considered for obtaining damper response. This exhibits a non-linear relationship between damper force and input-voltage/states, and hence obtaining the input voltage to realize a desired control force is a non-trivial task. Two voltage control laws are proposed, i.e. inverse quadratic voltage law (IQVL) and inverse On–off voltage law (IOOVL), both based on the MR constraint filter. These are implemented in addition to the existing clipped voltage law (CVL). Results for controlled response of the building are obtained in terms of peak and RMS values of response quantities (Interstorey Drift, Displacement, Acceleration). These are compared with existing results obtained via linear quadratic Gaussian (LQG) control using CVL, and via passive-on control with constant (saturation) voltage applied. A reduction in the maximum peak interstorey drift, maximum RMS interstorey drift, and performance index is obtained when using OSOF-IOOVL/CVL control as compared with passive-on control. These quantities as well as RMS storey displacements are attenuated when comparing OSOF-IOOVL/CVL control with LQG-CVL control, with the exception of maximum peak interstorey drift for which the attenuation occurs for IOOVL only. The peak and RMS values of accelerations are reduced via OSOF compared with passive-on/LQG-CVL control, except when considering first-storey accelerations using passive-on control. The peak value of the applied damper force is least when using OSOF control.

Received 12 November 2009; Revised 12 March 2010; Accepted 16 May 2010

KEY WORDS: optimal static output feedback; LQG; MR damper; Bouc–Wen model

1. INTRODUCTION

Semi-active systems are a class of active systems which have received much attention due to their low power requirements. These consist of devices such as Variable Orifice Dampers, Controllable Fluid (Electrorhelogical (ER)/MR) Dampers, Variable Stiffness Devices, etc., combined with optimal controller designs [1]. The magnetorheological (MR) damper is a semi-active device that uses MR fluids exhibiting controllable yield characteristics. It produces sizeable damping force for small input voltage as demonstrated by Spencer *et al.* [2].

Various nonparametric and parametric mathematical models have been developed to describe the behavior of ER/MR dampers. Notable among the nonparametric models for semi-active dampers are those of Ehrgott and Masri [3] and Song *et al.* [4]. In [3] a Tchebycheff

*Correspondence to: Naresh K. Chandiramani, Department of Civil Engineering, Indian Institute of Technology Bombay, Mumbai 400076, India.
†E-mail: naresh@civil.iitb.ac.in

polynomial fit for constant current and excitation frequency is used to predict the ER damper force. Force–velocity predictions agree well with the experiment during pre-yield, but oscillations occur during post-yield. A large number of polynomial terms are required to maintain accuracy. In [4] an MR damper is modeled using shape functions, polynomial function, and a first-order filter to capture the back bone, saturation behavior and hysteretic behavior, respectively. Current-dependent experimental data were used to obtain model parameters using constrained nonlinear optimization.

Parametric models are based on mechanical elements, i.e. friction, spring, damper, and hysterisis elements. A Bingham model was proposed by Stanway *et al.* [5], yielding good force–displacement behavior but poor force–velocity response due to the inability of the piecewise linear model to capture hysteretic behavior. The hysteretic force was modeled via an evolutionary variable and loop control parameters by Wen [6], giving rise to the class of Bouc–Wen models for MR dampers. Wong *et al.* [7] studied the influence of loop control parameters and obtained a wide variety of hysteresis loops, thus establishing the Bouc–Wen models versatility in matching experimental data, except near small velocities. This shortcoming was rectified by Spencer *et al.* [8] in their modified Bouc–Wen model. Therein, additional damping and stiffness elements were used to model the behavior at low velocities and the accumulator, respectively. The voltage-dependent model parameters were determined using test data for periodic/random displacement input and constant/random voltage input. Dominguez *et al.* [9] developed a current–frequency–amplitude dependent Bouc–Wen model along with a model identification method. Wang and Kamath [10] developed a phase-transition model using Lagrangian dynamics to obtain a second-order nonlinear differential equation for damper force with damper velocity as input. Jiménez and Álvarez-Icaza [11] modified the LuGre friction-based model [12] by replacing material dependency in the original model by voltage dependency, and including voltage dependency for the hysteresis component. Model identification was done for current-dependent parameters. Sakai *et al.* [13] included an additional hysteresis component and altered the voltage dependency, in order to obtain the inverse dynamics (i.e. voltage for given force).

Various methods for controller design have been used with MR dampers. Owing to the complexity in solving the inverse dynamical problem, predicting the applied voltage that would produce a desired damper force becomes a challenging task. Different voltage laws have been proposed to address this issue [14]. Xu and Shen [15] used Bi-state and Intelligent bi-state control strategies for seismic response reduction of a building, with a Bingham model for the MR damper. The applied damper force was produced via an on–off current law. A neural network-based prediction of response was done to reduce time delays. Dyke *et al.* [16] implemented acceleration feedback LQG control for a three-storey building with modified Bouc–Wen model for the MR damper. The desired damper force was obtained using measured output (i.e. accelerations and displacement) and measured damper force, thereby replacing the need for state estimation with an online numerical evaluation of a convolution integral. Control voltage was obtained via an on–off voltage law based on the desired and measured damper forces. Jansen and Dyke [17] compared various control strategies, i.e. Lyapunov control, Decentralized bang–bang control, Modulated homogeneous friction control and LQG control with acceleration feedback, using different voltage laws for each of these strategies.

Chang and Zhou [18] used LQR control for seismic response reduction in a building with the MR damper modeled using the modified Bouc–Wen model. The inverse dynamics of the damper were modeled with a recurrent neural network using a constraint filter, so as to obtain the required voltage for given damper force. Yuen *et al.* [19] used the reliability-based robust linear controller design with a modified Bouc–Wen model for the MR damper. Uncertainties in plant dynamics and excitation were considered, and a robust method involving probability distribution over a set of possible plant models was used to obtain the desired damper force. The command voltage is determined via the modified clipped voltage proposed by Yoshida and Dyke [20].

Most controller designs studied above are either based on full state feedback (which requires state measurement or estimation) or result in complex compensator structures. Optimal static

DOI: 10.1002/stc

output feedback (OSOF) control avoids observer design, has a simple compensator structure, and produces the control force desired based on few measurements of output. In this paper, OSOF control strategy is implemented for seismic response attenuation of a three-storey building with the MR damper modeled using the hysteresis-based modified Bouc–Wen model. Two voltage control laws are proposed based on an MR constraint filter. These are implemented along with the existing Clipped voltage law (CVL) so as to obtain the command voltage for a desired damper force.

2. SYSTEM MODEL

2.1. MR damper

The modified Bouc–Wen model is considered in order to include damper characteristics in the system model. This has been developed by Spencer *et al.* [8] for the prototype MR damper developed by Lord Corporation, U.S.A. Dependency of damper parameters on applied voltage v is included in this model. Figure 1 shows the schematic of the modified Bouc–Wen model.

The force f, as given by this model, is

$$f = c_1\dot{y}+k_1(x-x_0) \tag{1}$$

and

$$\dot{y} = \frac{1}{(c_0+c_1)}\{\alpha z+c_0\dot{x}+k_0(x-y)\} \tag{2}$$

where the evolutionary variable z is governed by

$$\dot{z} = -\gamma|\dot{x}-\dot{y}|z|z|^{n-1} - \beta(\dot{x}-\dot{y})|z|^n+A(\dot{x}-\dot{y}) \tag{3}$$

Here x, $\dot{x}$ and f are the damper displacement, velocity and force, respectively, k_1 is the accumulator stiffness, x_0 is the initial displacement of the spring k_1 which produces the nominal damper force due to the accumulator, c_0 is the viscous damping observed at large velocity, c_1 is the viscous damping at low velocity to take care of nonlinear roll-off, and the stiffness k_0 is used to emulate the stiffness at large velocities. The evolutionary variable z in Equation (2) describes the hysteretic behavior of the MR damper. Loop parameters γ and β affect the shape and A affects the slope of hysteresis loop, while n governs the smoothness of the transition from linear to non-linear range [7].

The voltage dependency of model parameters is given as [8]

$$\alpha = \alpha(u) = \alpha_a+\alpha_b u, \quad c_1 = c_1(u) = c_{1a}+c_{1b}u, \quad c_0 = c_0(u) = c_{0a}+c_{0b}u \tag{4}$$

where u is the output of a first-order filter that models the combined dynamics of the current driver and the fluid reaching rheological equilibrium, i.e.

$$\dot{u} = -\eta(u-v) \tag{5}$$

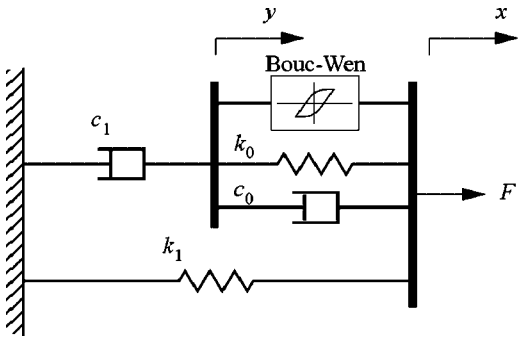

Figure 1. Modified Bouc–Wen model of the MR damper.

DOI: 10.1002/stc

Table I. Parameters for the generalized modified Bouc–Wen model [8].

Parameter	Value	Parameter	Value
c_{0a}	21.0 N s/cm	α_a	140 N/cm
c_{0b}	3.50 N s/cm V	α_b	695 N/cm · V
k_0	46.9 N/cm	γ	363 cm^{-2}
c_{1a}	283 N s/cm	β	363 cm^{-2}
c_{1b}	2.95 N s/cm V	A	301
k_1	5.00 N/cm	n	2
x_0	14.3 cm	η	190 s^{-1}

Here, v is the control input voltage to the current driver. The model parameter values as obtained by Spencer *et al.* [8], by optimal fitting of their model to experimental data, are shown in Table I.

2.2. MR constraint filter—proposed control law

The limits of the evolutionary variable z was obtained by Spencer [21] as:

$$z_u = \pm \left(\frac{A}{\gamma+\beta}\right)^{1/n} \tag{6}$$

Following Chang and Zhou [18] it can be numerically shown that the contribution of stiffness terms in Equations (1) and (2) is less than those of the damping terms, and hence they are neglected in the following. Using Equations (2) and (1), the bounds of the MR damper force f are approximated by:

$$f \approx \frac{c_1}{c_0+c_1}\{\alpha z_u + c_0\dot{x}\} \tag{7}$$

For a constant applied voltage v, the steady-state solution of Equation (5) is $u = v$. Substituting this in Equation (4) and then in Equation (7), the approximate damper force is [18]

$$f \approx \frac{(c_{1_a}+c_{1_b}v)}{[(c_{0_a}+c_{1_a})+(c_{0_b}+c_{1_b})v]}[(\alpha_a+\alpha_b v)z_u+(c_{0_a}+c_{0_b}v)\dot{x}] \tag{8}$$

Substituting the values of parameters from Table I into Equation (8), the minimum and maximum force $f_{\min}$ and $f_{\max}$ produced by the damper is obtained for applied voltage $v = 0$ V and $v = 2.25$ V, respectively. For any intermediate voltage the damper force varies linearly with velocity. This is represented by a straight line lying within the realizable force region defined by the two limiting straight lines (Figure 2). The realizable zone in the first and third quadrants is obtained for positive and negative values, respectively, of z_u. This is termed the MR constraint filter [18].

The control laws proposed herein are based on Equation (8) from which an inverse relation is obtained between the damper force and the applied voltage. Equation (8) yields

$$\begin{aligned}&\{c_{1_b}\alpha_b z_u + c_{1_b}c_{0_b}\dot{x}\}v^2 + \{(c_{1_a}\alpha_b + c_{1_b}\alpha_a)z_u + (c_{1_a}c_{0_b} + c_{1_b}c_{0_a})\dot{x} - (c_{0_b}+c_{1_b})f\}v \\ &\quad + \{c_{1_a}\alpha_a z_u + c_{1_a}c_{0_a}\dot{x} - (c_{0_a}+c_{1_a})f\} = 0\end{aligned} \tag{9}$$

The required voltage for a given desired control force f_d and velocity $\dot{x}$ can be obtained via Equation (9). The voltage predicted using z in place of z_u in Equation (9) would be more accurate but not implementable, as z is unmeasurable. The following two voltage control laws are proposed, based on the MR constraint filter, in order to obtain the control voltage to be applied. These control laws are easily implementable with linear quadratic optimal control algorithms that determine the desired optimal control force (i.e. the control input) f_d that is required to be supplied by the MR damper.

(1) *Inverse quadratic voltage law* (*IQVL*): If $\dot{x}f_d > 0$ and f_d obtained lies outside the realizable region of the MR constraint filter, then the control voltage is set to the appropriate limiting value, i.e. if $|f_d| > |f_{\max}|$ then $v = v_{\max} = 2.25$ V, else if $|f_d| < |f_{\min}|$ then $v = v_{\min} = 0$ V. If $\dot{x}f_d > 0$ and f_d obtained lies within the realizable region, i.e. $|f_{\min}| \leqslant |f_d| \leqslant |f_{\max}|$, the control voltage is

DOI: 10.1002/stc

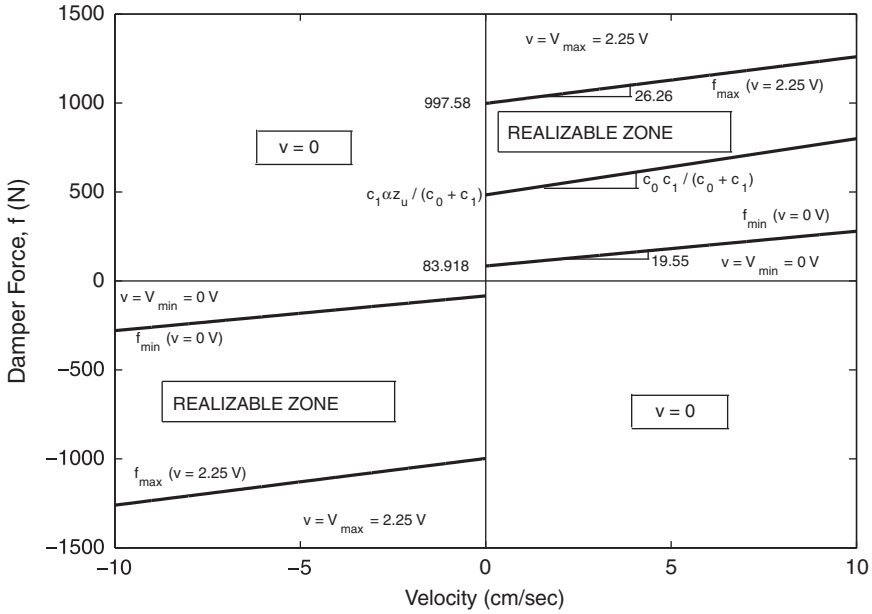

Figure 2. Realizable MR damper force zone in first and third quadrant of $f - \dot{x}$ plane.

obtained from Equation (9) by substituting f_d for f, and using positive z_u if $f_d > 0$, $\dot{x} > 0$ or negative z_u if $f_d < 0$, $\dot{x} < 0$. If $\dot{x} f_d < 0$ then $v = v_{\min} = 0\,\mathrm{V}$.

(2) *Inverse on–off voltage law* (*IOOVL*): This is same as IQVL except that $v = v_{\max} = 2.25\,\mathrm{V}$ even when f_d lies within the realizable zone. Thus, Equation (9) is not required in IOOVL.

The existing *clipped voltage law* (CVL) [16] is considered for the comparison with proposed IQVL and IOOVL. It uses f_d and f (applied damper force) in contrast to IQVL and IOOVL, which use f_d and $\dot{x}$. If $f_d f < 0$ then $v = v_{\min} = 0\,\mathrm{V}$; else $v = v_{\max} = 2.25\,\mathrm{V}$ when $|f_d| > |f|$, or $v = v_{\min} = 0\,\mathrm{V}$ when $|f_d| < |f|$, or v is held at its present value when $|f_d| = |f|$.

2.3. Structural model

One of the aims of the study is to compare OSOF control with LQG control applied by Dyke *et al.* [16]. Hence the simplified model of the test structure developed in [16], where masses are assumed to be lumped at floor levels, is chosen here. This is a three-storey building with a single MR damper attached between ground and first storey, shown in Figure 3.

The equation of motion is given by

$$\mathbf{M}_s\ddot{\mathbf{x}} + \mathbf{C}_s\dot{\mathbf{x}} + \mathbf{K}_s\mathbf{x} = \mathbf{G}\mathbf{f} - \mathbf{M}_s\mathbf{L}\ddot{x}_g \tag{10}$$

where $\mathbf{M}_s$, $\mathbf{C}_s$, and $\mathbf{K}_s$ are mass, damping, and stiffness matrices, respectively, $\mathbf{G}$ is the location matrix of the MR damper, $\mathbf{f}$ is the applied control force as defined by Equation (1), $\mathbf{L}$ is the location matrix of earthquake excitation, $\ddot{x}_g$ is the earthquake excitation, and $\mathbf{x} = [x_1 \quad x_2 \quad x_3]^{\mathrm{T}}$ is the displacement vector of the three storeys measured relative to ground. Here, x_1 is damper relative displacement, denoted x in Sections 2.1 and 2.2. For the building considered here, these matrices are [16]

$$\begin{aligned}
\mathbf{M}_s &= \begin{bmatrix} 98.3 & 0 & 0 \\ 0 & 98.3 & 0 \\ 0 & 0 & 98.3 \end{bmatrix} \mathrm{kg}, \quad \mathbf{C}_s = \begin{bmatrix} 175 & -50 & 0 \\ -50 & 100 & -50 \\ 0 & -50 & 50 \end{bmatrix} \frac{\mathrm{N\,sec}}{\mathrm{m}} \\
\mathbf{K}_s &= 10^5 \begin{bmatrix} 12.0 & -6.84 & 0 \\ -6.84 & 13.7 & -6.84 \\ 0 & -6.84 & 6.84 \end{bmatrix} \frac{\mathrm{N}}{\mathrm{m}}, \quad \mathbf{G} = \begin{bmatrix} -1 \\ 0 \\ 0 \end{bmatrix}, \quad \mathbf{f} = [f\,], \quad \mathbf{L} = \begin{bmatrix} 1 \\ 1 \\ 1 \end{bmatrix}
\end{aligned} \tag{11}$$

DOI: 10.1002/stc

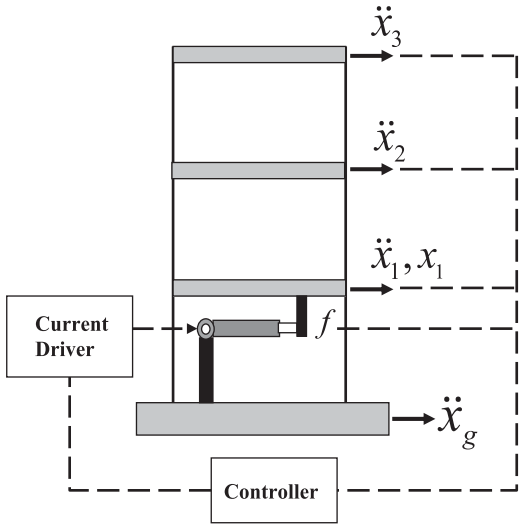

Figure 3. Three-storey building model with MR damper [16].

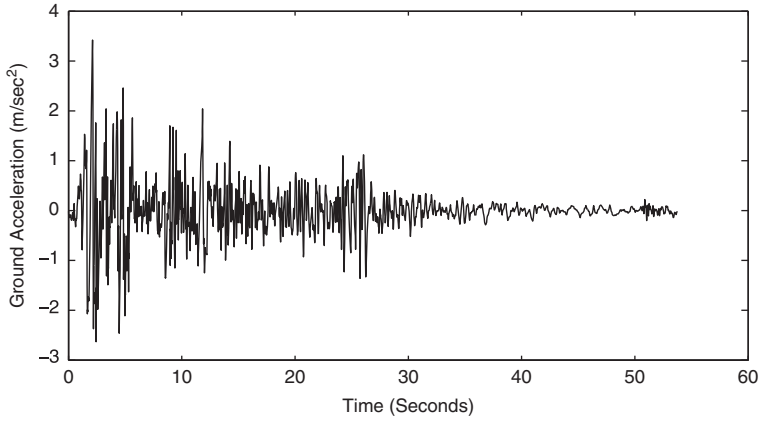

Figure 4. N-S component of El Centro ground acceleration data, Imperial Valley, 1940 [22].

Defining the state as $\mathbf{q} = [\mathbf{x} \;\; \dot{\mathbf{x}}]^{\mathrm{T}}$ and the output vector chosen as [16]

$$\mathbf{y} = [\ddot{x}_1 \;\; \ddot{x}_2 \;\; \ddot{x}_3 \;\; x_1]^{\mathrm{T}} = [\dot{q}_4 \;\; \dot{q}_5 \;\; \dot{q}_6 \;\; q_1]^{\mathrm{T}} \tag{12}$$

the state equations representing building dynamics (Equation (10)) and the output equation are

$$\dot{\mathbf{q}} = \mathbf{A}\mathbf{q} + \mathbf{B}\mathbf{f} + \mathbf{E}\ddot{x}_g \tag{13}$$

$$\mathbf{y} = \mathbf{C}\mathbf{q} + \mathbf{D}\mathbf{f} \tag{14}$$

where

$$\begin{aligned} \mathbf{A} &= \begin{bmatrix} \mathbf{0} & \mathbf{I} \\ -\mathbf{M}_s^{-1}\mathbf{K}_s & -\mathbf{M}_s^{-1}\mathbf{C}_s \end{bmatrix}, \quad \mathbf{B} = \begin{bmatrix} \mathbf{0} \\ \mathbf{M}_s^{-1}\mathbf{G} \end{bmatrix} \quad \mathbf{E} = -\begin{bmatrix} \mathbf{0} \\ \mathbf{L} \end{bmatrix} \\ \mathbf{C} &= \begin{bmatrix} -\mathbf{M}_s^{-1}\mathbf{K}_s & -\mathbf{M}_s^{-1}\mathbf{C}_s \\ 1 \;\; 0 \;\; 0 & 0 \;\; 0 \;\; 0 \end{bmatrix}, \quad \mathbf{D} = \begin{bmatrix} \mathbf{M}_s^{-1}\mathbf{G} \\ 0 \end{bmatrix} \end{aligned} \tag{15}$$

The MR damper dynamics is given by Equations (1)–(5). Damper parameters in Table I are used for numerical simulations, except x_0 which was set to zero, i.e. the initial offset due to the accumulator is neglected [16]. The building is subjected to N-S component of the 1940 El Centro ground acceleration motion measured at Imperial Valley as shown in Figure 4 [22]. Since the

DOI: 10.1002/stc

building is a scaled model, the time scale of ground motion data is scaled down by five times the recorded rate.

3. STATIC OUTPUT FEEDBACK CONTROL

The state variables are often not measurable for feedback. One way to design the controller in such situations is by designing an observer (i.e. state estimator) and then using an observer-based feedback. The Luenberger observer uses the measured output and control input to estimate the states which are then fed back, i.e. the control input is obtained from the estimated states. Linear quadratic Gaussian (LQG) control algorithm [23] can be used when noise is present in output measurement and structural system (i.e. plant) dynamics. This involves state estimation via a Kalman filter which minimizes the error made in state estimation by the Luenberger observer.

Alternatively, the controller design can be done without state estimation, i.e. by obtaining the desired control input (MR damper force in this case) via measured output feedback instead of state feedback. This is termed Linear quadratic regulator (LQR) with Output feedback or OSOF control. This has the advantage of fewer on-line computations as compared with LQG control.

Consider the structural system dynamics given by state equations

$$\dot{\mathbf{q}} = \mathbf{A}\mathbf{q} + \mathbf{B}\mathbf{f}_d \tag{16}$$

and the measured output equation

$$\mathbf{y} = \mathbf{C}\mathbf{q} \tag{17}$$

Here, $\mathbf{f}_d$ is the desired damper force, i.e. the control input obtained by output feedback as

$$\mathbf{f}_d = -\mathbf{K}\mathbf{y} \tag{18}$$

where $\mathbf{K}$ is the matrix of constant feedback gains to be determined. In OSOF regulator design $\mathbf{K}$ and hence $\mathbf{f}_d$ are determined such that the quadratic performance index (PI) defined as

$$J^* = \frac{1}{2}\int_0^\infty [\mathbf{q}^{\mathrm{T}}\mathbf{Q}\mathbf{q} + \mathbf{f}_d^{\mathrm{T}}\mathbf{R}\mathbf{f}_d]\,\mathrm{d}t \tag{19}$$

is minimized. Here, $\mathbf{Q}$ is the positive semi-definite state weighting matrix and $\mathbf{R}$ is the positive-definite control input weighting matrix. In general, if the controller is effective for random initial conditions it is also effective for random input excitations [24]. Following Lewis and Syrmos [23], Equations (16)–(18) yield the closed-loop system equation,

$$\dot{\mathbf{q}} = (\mathbf{A} - \mathbf{B}\mathbf{K}\mathbf{C})\mathbf{q} = \mathbf{A}_c\mathbf{q} \tag{20}$$

The PI can be expressed in terms of $\mathbf{K}$ using Equations (17)–(19) as

$$J^* = \frac{1}{2}\int_0^\infty [\mathbf{q}^{\mathrm{T}}(\mathbf{Q} + \mathbf{C}^{\mathrm{T}}\mathbf{K}^{\mathrm{T}}\mathbf{R}\mathbf{K}\mathbf{C})\mathbf{q}]\mathrm{d}t \tag{21}$$

If a constant, symmetric, positive semi-definite matrix $\mathbf{P}$ exists such that

$$\frac{\mathrm{d}}{\mathrm{d}t}(\mathbf{q}^{\mathrm{T}}\mathbf{P}\mathbf{q}) = -\mathbf{q}^{\mathrm{T}}(\mathbf{Q} + \mathbf{C}^{\mathrm{T}}\mathbf{K}^{\mathrm{T}}\mathbf{R}\mathbf{K}\mathbf{C})\mathbf{q} \tag{22}$$

then Equations (20) and (22) yield a Lyapunov equation for $\mathbf{P}$ (assuming $\mathbf{K}$ is known), i.e.

$$\mathbf{g} \equiv \mathbf{A}_c^{\mathrm{T}}\mathbf{P} + \mathbf{P}\mathbf{A}_c + \mathbf{C}^{\mathrm{T}}\mathbf{K}^{\mathrm{T}}\mathbf{R}\mathbf{K}\mathbf{C} + \mathbf{Q} = \mathbf{0} \tag{23}$$

Using Equations (21) and (22), considering an asymptotically stable closed-loop system ($\mathbf{q} \to 0$ as $t \to \infty$), and noting that the scalar PI equals its own trace and that the product in a trace is commutable, the PI becomes

$$J^* = \tfrac{1}{2}\mathbf{q}^{\mathrm{T}}(0)\mathbf{P}\mathbf{q}(0) = \tfrac{1}{2}\mathrm{tr}(\mathbf{P}\tilde{\mathbf{Q}}) \tag{24}$$

where $\tilde{\mathbf{Q}} \equiv \mathbf{q}(0)\mathbf{q}^{\mathrm{T}}(0)$. The optimization problem is to determine the gain $\mathbf{K}$ that minimizes the PI in Equation (24) subject to the constraint Equation (23). Thus, the Hamiltonian defined as

DOI: 10.1002/stc

$\mathbf{H} = \text{tr}(\mathbf{P}\tilde{\mathbf{Q}}) + \text{tr}(\mathbf{gS})$ is minimized with respect to $\mathbf{P}$, $\mathbf{S}$, and $\mathbf{K}$, where $\mathbf{S}$ is the matrix of Lagrange multipliers. This yields the design equations [23]:

$$\mathbf{A}_c\mathbf{S} + \mathbf{S}\mathbf{A}_c^{\mathrm{T}} + \tilde{\mathbf{Q}} = \mathbf{0} \tag{25}$$

$$\mathbf{R}^{-1}\mathbf{B}^{\mathrm{T}}\,\mathbf{P}\mathbf{S}\mathbf{C}^{\mathrm{T}}\,(\mathbf{C}\mathbf{S}\mathbf{C}^{\mathrm{T}})^{-1} = \mathbf{K} \tag{26}$$

along with the constraint Equation (23) recovered. Equations (23) and (25) are Lyapunov equations in unknowns $\mathbf{P}$ and $\mathbf{S}$, respectively, and Equation (26) gives the optimal gain $\mathbf{K}$. Equations (23), (25), (26) represent a coupled nonlinear system of matrix equations in the unknowns and depend on initial conditions. In order to eliminate the dependency on initial conditions, the PI is replaced by its expected value [25]. This amounts to replacing $\tilde{\mathbf{Q}}$ by its expected value (i.e. $\tilde{\mathbf{Q}} = E\{\mathbf{q}(0)\mathbf{q}^{\mathrm{T}}(0)\}$—the initial autocorrelation of the state) in Equation (25). Assuming that initial states are uniformly distributed on the unit sphere [25] implies that $\tilde{\mathbf{Q}} = \mathbf{I}$ in Equation (25), where $\mathbf{I}$ is the identity matrix. The optimal cost thus becomes [23]

$$E[J^*] = J = \tfrac{1}{2}\,\text{tr}[\mathbf{P}] \tag{27}$$

Various iterative algorithms are available to solve Equations (23), (25), (26) to obtain the optimal gain $\mathbf{K}$ [23]. The algorithm of Moerder and Calise [26], used here, is as follows:

Step (1): Initialization: Iteration counter $k = 0$, $\tilde{\mathbf{Q}} = \mathbf{I}$. Select the initial output feedback gain $\mathbf{K}_0$ so that $\mathbf{A}_c$ is asymptotically stable. If open-loop plant is stable, then $\mathbf{K}_0 = 0$ can be the choice.

Step (2): $\mathbf{A}_k \leftarrow (\mathbf{A} - \mathbf{B}\mathbf{K}_k\mathbf{C})$, $\mathbf{A}_c \leftarrow \mathbf{A}_k$, $\mathbf{K} \leftarrow \mathbf{K}_k$. Solve Equations (23) and (25) for $\mathbf{P}$ and $\mathbf{S}$. $\mathbf{P}_k \leftarrow \mathbf{P}$, $\mathbf{S}_k \leftarrow \mathbf{S}$, $J_k = \frac{1}{2}\text{tr}[\mathrm{P}_k]$. If $k > 0$ and $|J_k - J_{k-1}| < \varepsilon$, where ε is a small tolerance, algorithm has converged, go to Step 4.

Step (3): $\mathbf{K}_{k+1} \leftarrow \mathbf{K}_k + \alpha\Delta\mathbf{K}$, where $\Delta\mathbf{K} = \mathbf{R}^{-1}\mathbf{B}^{\mathrm{T}}\mathbf{P}_k\mathbf{S}_k\mathbf{C}^{\mathrm{T}}(\mathbf{C}\mathbf{S}_k\mathbf{C}^{\mathrm{T}})^{-1} - \mathbf{K}_k$ and α is chosen : $\mathbf{A}_{k+1}$ is asymptotically stable where $\mathbf{A}_{k+1} \leftarrow (\mathbf{A} - \mathbf{B}\mathbf{K}_{k+1}\mathbf{C})$. $k \leftarrow k+1$. Go to Step (2).

Step (4): $\mathbf{K} = \mathbf{K}_k$

In the presence of a feed-through (i.e. direct transmission) term $\mathbf{D}\mathbf{f}_d$, as in the present case, the measured output is

$$\hat{\mathbf{y}} = \mathbf{C}\mathbf{q} + \mathbf{D}\mathbf{f}_d \tag{28}$$

Hence the control input, i.e. desired damper force, obtained via output feedback is

$$\mathbf{f}_d = -\mathbf{K}\hat{\mathbf{y}} \tag{29}$$

From Equations (28) and (29) one obtains

$$\mathbf{f}_d = -\hat{\mathbf{K}}\mathbf{y} \quad \text{where} \quad \hat{\mathbf{K}} = (\mathbf{I} + \mathbf{K}\mathbf{D})^{-1}\,\mathbf{K} \tag{30}$$

Equation (30) is equivalent to Equation (18) with $\mathbf{K}$ replaced by $\hat{\mathbf{K}}$. The optimal feedback gain $\hat{\mathbf{K}}$ can be obtained by the Moerder–Calise algorithm. Subsequently, the feedback gain $\mathbf{K}$ is obtained as

$$\mathbf{K} = \hat{\mathbf{K}}(\mathbf{I} - \mathbf{D}\hat{\mathbf{K}})^{-1} \tag{31}$$

for use in actual implementation in the controller. Previous implementations of OSOF control do not consider the feed-through term [24]. Hence they are restricted to measured outputs being combinations of states alone, i.e. desired control force is obtained from displacement and velocity feedback only. Since the feed-through term is considered herein, in a practical implementation the desired control force can be obtained using acceleration feedback also, as done here.

Equations (1)–(5) show that the force f generated by the damper is nonlinearly dependent on the state vector $(\mathbf{q}^{\mathrm{T}}\, y\; z\; u)^{\mathrm{T}}$ and input voltage. Thus the inverse problem, i.e. determining the individual voltages to be applied to a set of MR dampers so as to produce the desired control force vector $\mathbf{f}_d$ for a given state vector, is difficult to solve by conventional methods. Since only the voltage v applied to each MR damper can be commanded by the controller, the desired force $\mathbf{f}_d$ is difficult to achieve in practice. Thus, the applied voltage is decided by the voltage control laws such as IQVL, IOOVL, proposed herein, and CVL [16]. The block diagram of the physical implementation of OSOF control algorithm is shown in Figure 5. Here, the damper velocity is equivalently denoted as $\dot{x} \equiv \dot{x}_1 \equiv q_4$. It is considered to be measured using a velocity sensor, for

DOI: 10.1002/stc

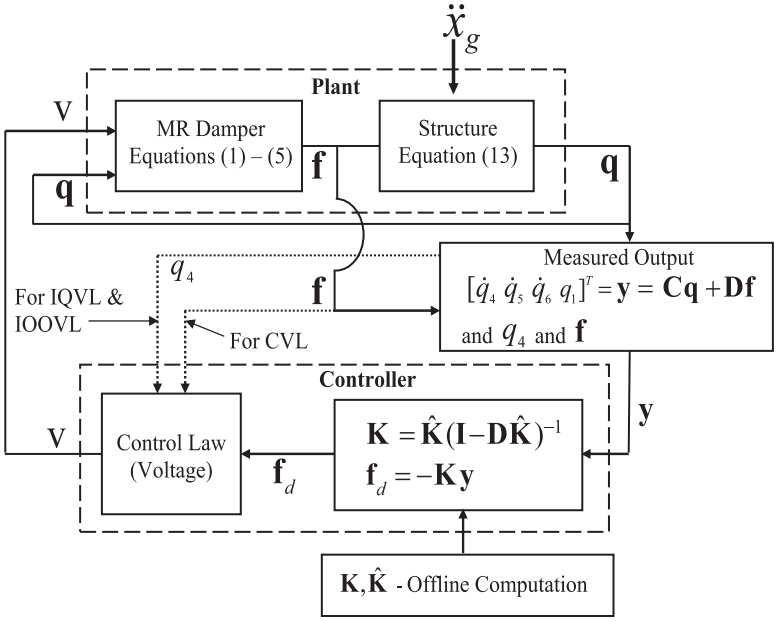

Figure 5. Implementation of optimal static output feedback control algorithm.

use in the control law. Although it is a measured output, it is not included in **y** as it is not used to obtain f_d herein (i.e. it is neither used in the estimator design in LQG control nor in the output feedback part of OSOF control). However, this does not preclude it from being a part of **y** in future applications. Note that the LQG control in [27] uses the same **y** as done herein, and hence can be easily compared with the present OSOF results.

As noted earlier, LQG control is based on full state feedback, i.e. in controller design the desired force is computed using the complete state vector ($f_d = \mathbf{Kq}$). Since the complete state vector is usually not measurable, its estimate is used in order to generate the f_d to be supplied to the control-law (Figure 5). The state estimator (observer) uses the measured output **y** as its input, and becomes an additional part of the controller, which needs to be designed. In contrast, in output feedback controller design, f_d is computed directly (Equation 18) by using the measured output **y** (Equation (12)), without using an estimator as a part of the controller (Figure 5). The components of **y** are directly measured from the physical system (i.e. building herein), are chosen as readily measurable quantities (i.e. accelerations of the three storeys and displacement of the first storey herein), and are invariably fewer than the number of states.

4. RESULTS AND DISCUSSIONS

The three-storey building subjected to earthquake excitation (Section 2.3) has been studied using MATLAB. The following cases are considered:

(1) Passive Control: For the passive-off case no voltage is applied to the damper, i.e. $v = 0$ V. For the passive-on case the damper force saturation voltage $v = 2.25$ V is applied.
(2) Semi-active Control: The desired control force $\mathbf{f}_d$ (i.e. control input vector) is determined using either LQG or OSOF control method. Then the voltage applied to the damper is obtained, using $\mathbf{f}_d$, via either of the voltage laws (i.e. IQVL, IOOVL and CVL).

If the voltage law is not specified with the control method it is implied that the result pertains to any of the three voltage laws used with the particular control method.

The first-order ODE's (Equations (2), (3), (5)) pertaining to the MR damper and state equations pertaining to the structural system dynamics (Equation (13)) were simultaneously

DOI: 10.1002/stc

solved using MATLAB module ODE45 (i.e. the 4th/5th-order Runge–Kutta method). Initial conditions are $\mathbf{q}(0) = 0$ (structure at rest), $u(0) = 0$ (no applied voltage), $z(0) = 0$ (no hysterisis component), and $y(0) = 0$ (no relative motion of damper model components). Without loss of generality, the accumulator spring is assumed initially undeformed ($x_0 = 0$) [27]. Peak and RMS values of response quantities like interstorey drift, displacement, and acceleration are obtained to assess the controller performance. Results using passive control and LQG-CVL control are compared with the similar ones available in Dyke *et al.* [27]. The peak response quantities occurring during the earthquake are in good agreement as seen from Table II where percentage difference indicated below respective quantities.

4.1. Peak response

The OSOF controllers are compared with the passive and LQG-CVL controllers in Table III for storey-wise peak values of interstorey drift, displacement, and acceleration, as well as performance index and peak damper force. The PI used contains only top floor acceleration apart from control input. Hence, $\mathbf{Q} = \mathbf{C}^{\mathrm{T}}\hat{\mathbf{Q}}\mathbf{C}$ where $\hat{\mathbf{Q}}$ is the null matrix with $\hat{Q}_{33} = 1$. For a single damper, the control input (i.e. damper force vector) is a scalar and hence the corresponding weighting matrix is $\mathbf{R} = [R]$. The value of R indicated in the tables for the semi-active controllers (i.e. LQG and OSOF) corresponds to most effective control for the particular combination of control method and voltage law. The PI reported for passive-on control is shown alongside the corresponding semi-active PI since both PI's are evaluated using the same $\mathbf{Q}$ and R value for easy comparison.

Table III shows a substantial reduction of 61.43 and 71.30% in the maximum peak interstorey drift using passive-off and passive-on control, respectively, as compared with uncontrolled response obtained without the MR damper. The corresponding displacements and accelerations also show a similar reduction, e.g. for the third floor, the reduction in peak displacement is 53.14 and 68.65%, while the reduction in peak acceleration is 48.55 and 45.51% when using passive-off and passive-on control, respectively. It is observed that passive-on control increases the second- and third-storey accelerations as compared with passive-off control. The peak MR damper force is 3.7 times larger for passive-on control vis-a-vis passive-off control.

Table II. Comparison of results for uncontrolled, passive and LQG-CVL.

Control strategy	Uncontrolled		Passive off		Passive on		LQG-CVL	
	Dyke *et al.*	Present	Dyke *et al.*	Present	Dyke *et al.*	Present	Dyke *et al.*	Present
Displacement (cm)	0.538	0.547	0.211	0.211	0.076	0.079	0.114	0.1204
		1.67%		**0%**		**3.95%**		**5.61%**
	0.82	0.835	0.357	0.357	0.196	0.1952	0.185	0.1876
		1.83%		**0%**		**−0.41%**		**1.41%**
	0.962	0.971	0.455	0.455	0.306	0.3044	0.212	0.2177
		0.94%		**0%**		**−0.53%**		**2.69%**
Interstorey drift (cm)	0.538	0.547	0.211	0.211	0.076	0.079	0.114	0.1204
		1.67%		**0%**		**3.95%**		**5.61%**
	0.319	0.318	0.153	0.154	0.158	0.157	0.09	0.098
		−0.31%		**0.65%**		**−0.64%**		**8.89%**
	0.201	0.202	0.103	0.104	0.11	0.11	0.101	0.106
		0.50%		**0.97%**		**0%**		**4.95%**
Acceleration (cm/s^2)	856	873.69	420	397.36	281	273.96	696	757.4
		2.07%		**−5.70%**		**−2.57%**		**8.82%**
	1030	1069.4	480	489.48	494	495.96	739	733.08
		3.83%		**1.98%**		**0.40%**		**−0.81%**
	1400	1408	717	724.44	767	767.15	703	735.37
		0.57%		**1.04%**		**0.02%**		**4.60%**
MRD force (N)	—	—	258	258.97	979	964.69	941	969.72
				0.38%		**−1.48%**		**3.05%**

DOI: 10.1002/stc

Table III. Peak response, passive and semi-active control, El Centro ground motion.

Control strategy	Displacement (cm)	Interstorey drift (cm)	Acceleration (cm/s^2)	MRD force (N)	PI semi-active	PI passive on
Uncontrolled	0.547	0.547	873.69			
	0.835	0.318	1069.4	—	—	—
	0.971	0.202	1408			
Passive off	0.211	0.211	397.36			
	0.357	0.154	489.48	258.97	—	—
	0.455	0.104	724.44			
Passive on	0.079	0.079	273.96			
	0.1952	0.157	495.96	964.69	—	—
	0.3044	0.11	767.15			
LQG–CVL $R = 10^{-17}$	0.1204	0.1204	757.4			
	0.1876	0.098	733.08	969.72	7.007	8.521
	0.2177	0.106	735.37			
LQG–IQVL $R = 10^{-17}$	0.1181	0.1181	752.07			
	0.1847	0.0962	708.83	982.74	7.096	8.521
	0.2109	0.102	710.51			
LQG–IOOVL $R = 10^{-15}$	0.1139	0.1139	683.25			
	0.1808	0.096	708.83	982.74	7.327	8.521
	0.2109	0.102	710.51			
OSOF–CVL $R = 10^{-17}$	0.1203	0.1203	711.19			
	0.1739	0.100	383.19	809.21	5.2378	8.521
	0.2392	0.0796	553.86			
OSOF–IQVL $R = 10^{-06}$	0.1299	0.1299	693.92			
	0.1863	0.1112	457.36	768.43	5.498	8.729
	0.2509	0.0788	548.28			
OSOF–IOOVL $R = 10^{-08}$	0.1149	0.1149	783.01			
	0.1578	0.1033	438.1	905.79	5.5149	8.523
	0.2277	0.0797	554.58			

Table III shows that the maximum peak interstorey drift obtained by OSOF-IQVL control is attenuated by 38.44 and 17.26% when compared with passive-off and passive-on control, respectively. The corresponding attenuation for OSOF-CVL is 43 and 23.38%, respectively, and for OSOF-IOOVL is 45.55 and 26.82%, respectively. Thus, OSOF control provides substantial attenuation in the maximum peak interstorey drift vis-a-vis passive control.

Peak displacements and accelerations using OSOF control are substantially attenuated when compared with passive control, except for the first storey where the damper is attached. For example, the peak displacement of the top storey is reduced by 49.96 and 25.20% using OSOF-IOOVL as compared with passive-off and passive-on control, respectively. The corresponding reductions in peak accelerations are 23.45 and 27.71%, respectively.

The peak damper force applied as well as the PI are the lowest due to OSOF control as compared with passive-on/LQG control.

It can be seen from Table III that OSOF-IOOVL control results in lower maximum peak interstorey drift and lower peak displacements as compared with OSOF-IQVL/OSOF-CVL control.

When comparing the OSOF-IOOVL controller with the existing LQG-CVL controller, using the former reduces the maximum peak interstorey drift by 4.57% and peak displacements of first and second floor by 4.57 and 15.88%, respectively. However, it increases peak displacement of third floor by 4.39%. The corresponding peak accelerations of the second and third storey are substantially reduced by 40.24 and 24.58%, respectively, while that of the first storey increases marginally by 3.27%. Thus, the OSOF-IOOVL controller reduces the maximum interstorey drift when compared with the passive/LQG-CVL controller. Moreover, the LQG controller with the proposed IQVL and IOOVL (based on MR constraint filter) achieves marginally lower peak interstorey drift, peak displacement and peak acceleration for each storey as compared with LQG-CVL control.

Figure 6 shows the comparison of peak interstorey drift for passive-on, LQG-CVL, and OSOF-IOOVL control. Although the passive-on controller is effective in substantially reducing

DOI: 10.1002/stc

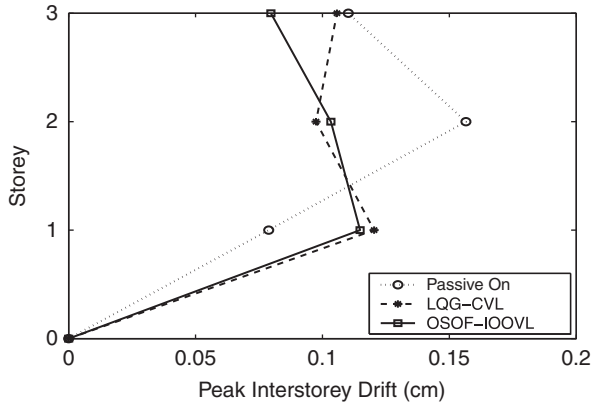

Figure 6. Peak interstorey drifts.

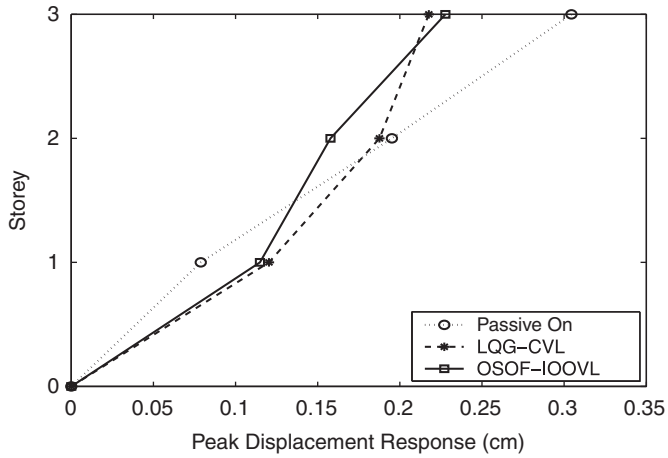

Figure 7. Peak storey displacements.

the peak interstorey drift at the first storey (where the MR damper is installed) vis-a-vis both semi-active controllers, the corresponding reduction at the remaining storeys is not as good. OSOF-IOOVL control clearly outperforms LQG-CVL control in this regard (as is seen by the max-peak and third-storey values) and both semi-active controllers perform much better than the passive-on controller as they tend to keep the interstorey drift uniformly low at all storeys.

Figures 7 and 8 show the comparison of peak displacements and accelerations for passive-on, LQG-CVL, and OSOF-IOOVL control. The semi-active controllers provide a reduction in peak displacement for the floors without the MR damper, the reduction being more prominent for OSOF control. The passive-on case shows a substantial reduction in peak accelerations vis-a-vis the uncontrolled system. As compared with passive-on control, the semi-active controllers yield substantially higher accelerations for the first floor (where the damper is attached). This is a result of the fact that the PI optimized by both the semi-active controllers contains the top storey acceleration. However, for the storeys without the damper, OSOF-IOOVL control appears very effective in controlling accelerations as compared with passive-on and LQG-CVL control, with the latter being least effective in this regard.

4.2. RMS response

The OSOF controllers are compared with the passive and LQG-CVL controllers in Table IV for storey-wise RMS values of interstorey drift, displacement, and acceleration, and the MR damper force.

DOI: 10.1002/stc

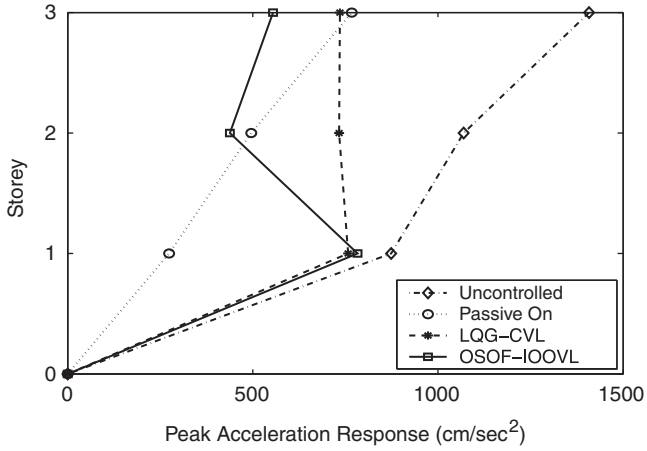

Figure 8. Peak storey acceleration.

Table IV. RMS response, passive and semi-active control, El Centro ground motion.

Control strategy	Displacement (cm)	Interstorey drift (cm)	Acceleration (cm/s^2)	MRD force (N)
Uncontrolled	0.2282	0.2282	304.59	
	0.3614	0.134	428.84	—
	0.4352	0.0756	526.26	
Passive off	0.0642	0.0642	94.839	
	0.1038	0.0411	136.35	103.35
	0.1263	0.0237	164.98	
Passive on	0.0182	0.0182	56.919	
	0.0409	0.0300	99.101	203.82
	0.0577	0.0188	130.54	
LQG–CVL $R = 10^{-17}$	0.0325	0.0325	90.655	
	0.0491	0.0225	124.15	156.33
	0.0599	0.017	118.38	
LQG–IQVL $R = 10^{-17}$	0.0326	0.0326	91.99	
	0.0494	0.0227	124.52	156.64
	0.0604	0.0171	119.13	
LQG–IOOVL $R = 10^{-15}$	0.0324	0.0324	87.57	
	0.0491	0.0227	133.03	156.35
	0.0600	0.0174	121.06	
OSOF–CVL $R = 10^{-17}$	0.0289	0.0289	92.93	
	0.0458	0.0235	85.17	163.31
	0.0578	0.0147	102.35	
OSOF–IQVL $R = 10^{-06}$	0.0316	0.0316	88.73	
	0.0499	0.0242	88.61	155.32
	0.0622	0.0149	103.71	
OSOF–IOOVL $R = 10^{-08}$	0.0254	0.0254	87.266	
	0.0421	0.0242	86.1	174.86
	0.0526	0.0151	105.01	

When compared with the uncontrolled response, the maximum RMS interstorey drift shows a substantial reduction of 71.87 and 86.85% for passive-off and passive-on control, respectively. Similar reductions occur in RMS values of displacements and accelerations of all storeys, e.g. the top floor RMS displacement reduces by 70.98 and 86.74% and corresponding RMS acceleration reduces by 68.65 and 75.19% for passive-off and passive-on control, respectively.

Comparisons of various OSOF controllers with passive-off and passive-on control, for maximum RMS interstorey drift, show reductions of 54.98 and 3.67%, respectively, when using OSOF-CVL, and 60.44 and 15.33%, respectively, when using OSOF-IOOVL. For OSOF-IQVL, the maximum RMS interstorey drift reduces by 50.77% but increases by 5.33% vis-a-vis

DOI: 10.1002/stc

passive-off and passive-on control, respectively. This again shows that OSOF-IOOVL is the most effective among the output feedback controllers Contrary to results for peak displacements, semi-active control results in higher RMS displacements as compared with passive-on control, with the exception of OSOF-IOOVL that provides an 8.83% reduction for the third storey. The corresponding comparison with passive-off control shows OSOF to be more effective for all storeys, e.g. the reduction is 58.35% for the top storey with OSOF-IOOVL control. For the storeys without the damper, OSOF yields attenuation in RMS accelerations as compared with passive control, e.g. for the third storey OSOF-IOOVL provides 36.35 and 19.56% attenuation when compared with passive-off and passive-on control, respectively.

Although the RMS damper force is lower via OSOF vis-a-vis passive-on control, it is higher vis-a-vis LQG control. A reduction in the maximum RMS interstorey drift and storey-wise RMS displacement is obtained via OSOF-IOOVL as compared with OSOF-IQVL/OSOF-CVL control. A reduction in the maximum RMS interstorey drift as well as storey-wise RMS displacement (except for IQVL) is obtained via OSOF as compared with LQG. For example, the reduction is 21.85% for the maximum RMS interstorey drift and 12.19% for RMS displacement of third storey when using OSOF-IOOVL vis-a-vis LQG-CVL control. The storey-wise RMS accelerations also show a reduction when OSOF-IOOVL is used vis-a-vis LQG-CVL, e.g. the reduction is 11.29% for the third storey.

Thus, the OSOF controller (in particular OSOF-IOOVL, and except OSOF-IQVL) is capable of subtantially reducing—the maximum RMS interstorey drift vis-a-vis passive/LQG control, the RMS displacements vis-a-vis LQG control, and the accelerations vis-a-vis passive/LQG control (except for the storey with damper for passive-on control).

4.3. Time history

Figure 9 shows the comparison of interstorey drift at storeys exhibiting maximum peak interstorey drift, i.e. at second storey using passive-on control and at first storey using LQG-CVL and OSOF-IOOVL control. The peak interstorey drift occurs at 0.44 s for passive-on control, 0.556 s for LQG-CVL, and 1.072 s for OSOF-IOOVL control. It is evident that OSOF-IOOVL control yields the lowest peak and RMS interstorey drift.

Figure 10 shows the accelerations of the third storey. The peak acceleration occurs at 0.45 s for all controllers. It can be seen that OSOF-IOOVL control yields the lowest peak and RMS acceleration as compared with Passive-on and LQG-CVL control.

Figure 11(a) shows the time history of voltage applied to the damper. The applied voltage switches between minimum ($v = 0$ V) and saturation ($v = 2.25$ V) levels when using OSOF-IOOVL control. Desired and applied damper forces are compared in Figure 11(b) and (c) where they are shown versus time and versus relative velocity (of damper), respectively. The differences between applied and desired damper forces are apparent in these figures. Figure 11(c) clearly shows that the applied damper force lies mostly in the first and third quadrant (a behavior that is inherent in

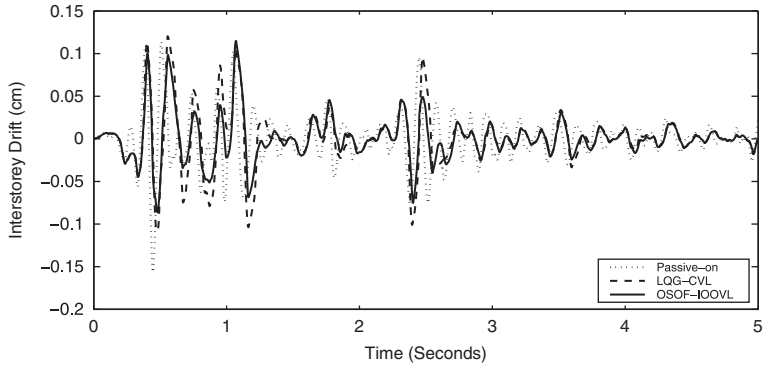

Figure 9. Time histories of interstorey drift corresponding to storey with maximum peak value; passive-on, LQG-CVL, OSOF-IOOVL control.

DOI: 10.1002/stc

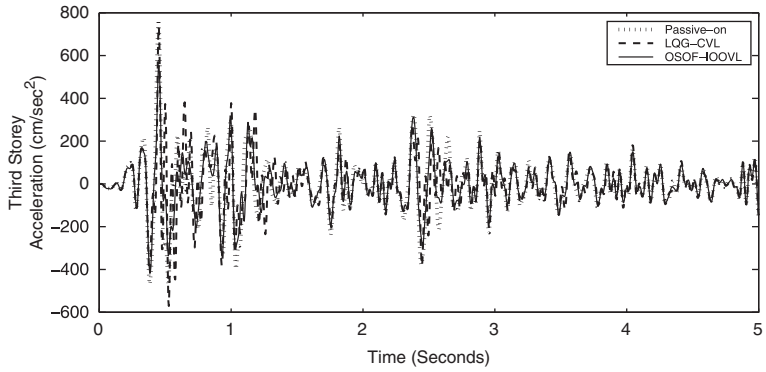

Figure 10. Time histories of third floor acceleration; passive-on, LQG-CVL, OSOF-IOOVL.

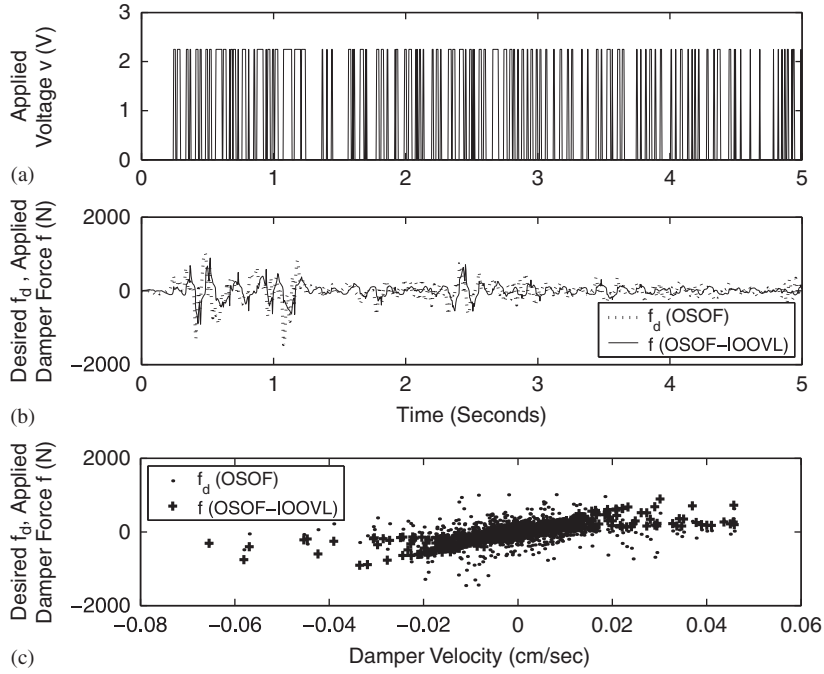

Figure 11. Time histories of (a) applied voltage; (b) desired, applied damper force; and (c) desired, applied damper force versus velocity; OSOF-IOOVL.

the damper constitutive law), whereas the desired damper force (obtained from the optimal controller) lies in all quadrants. This difference is due to two reasons; first the inverse dynamics of the damper (i.e. prediction of applied voltage for given force) is difficult to obtain, due to which the IOOVL has been considered in order to obtain the voltage approximately; second the damper force saturates at $v = 2.25$ V, which limits the maximum force that the damper can produce. The RMS difference between desired and applied damper forces is 259.02 N, which justifies the IOOVL as a reasonable alternative to exactly predicting the inverse dynamics.

Figure 12(a)–(c) shows time histories for interstorey drift at first storey, displacement at third storey, and acceleration at third storey, respectively, for uncontrolled and OSOF-IOOVL controlled response. These represent the storeys at which the interstorey drift, displacement, and acceleration are maximum for the uncontrolled structure (Table III). The peak values of interstorey drift, displacement, and acceleration occur at 1.072 s, 0.456 s, and 0.452 s, respectively, for OSOF-IOOVL control, and at 1.66 s, 1.66 s, and 0.936 s, respectively, for the uncontrolled case. The OSOF-IOOVL clearly yields a substantial reduction in peak and RMS quantities.

DOI: 10.1002/stc

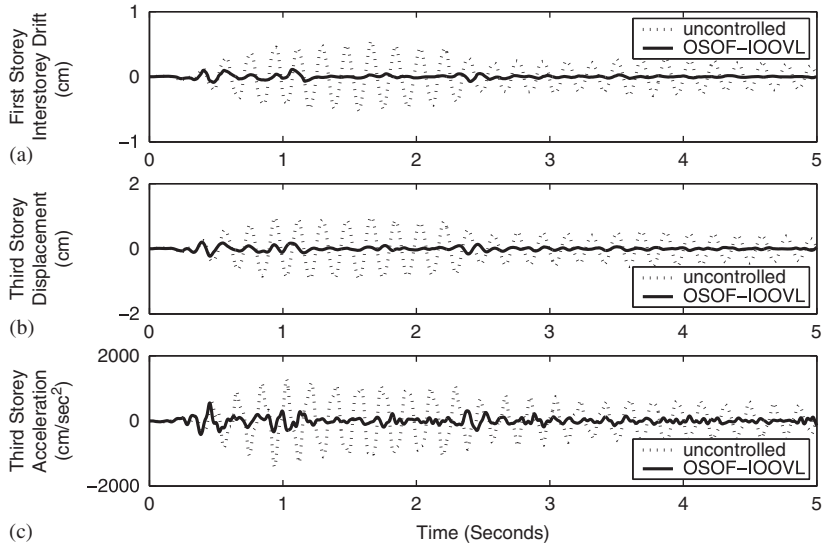

Figure 12. Time histories of (a) interstorey drift; (b) displacement; and (c) acceleration; uncontrolled and OSOF-IOOVL.

It is known that the optimal LQR control with full state feedback provides lower overshoot and settling time. Hence for pulse type ground motions, such as Northridge, which would be more amenable to control, it is expected that the performance of both semi-active optimal controllers vis-a-vis passive-on control will be further enhanced, as compared to when El-Centro ground excitation is considered. However, the comparison between the two semi-active controllers would need to be re-assessed.

5. CONCLUSIONS

An OSOF controller is used to determine the desired force (control input) required from an MR damper attached between ground and first storey for seismic response reduction of a three-storey building. A modified Bouc–Wen damper model is used. Since inverse dynamics of the damper is difficult to obtain, two voltage laws (IQVL and IOOVL) relating state and desired force to applied voltage are proposed using the MR constraint filter concept. Performance of the OSOF controller using these voltage laws is compared with that of existing passive/LQG-CVL controllers.

OSOF-IOOVL control yields lowest maximum peak interstorey drift when compared with passive/ LQG-CVL control. The maximum RMS interstorey drift obtained via OSOF control (except IQVL) is lowest when compared with passive/LQG control. OSOF control (except IQVL) yields reduced storey-wise RMS displacement as compared with LQG control. However, the opposite is mostly true when comparing with passive-on control. Peak and RMS values of accelerations are reduced via OSOF control compared with Passive-on/LQG-CVL control, except for first-storey accelerations when using passive-on control. Peak applied damper forces are lowest via OSOF control compared with passive-on/LQG control. However, the corresponding RMS value is higher when compared with LQG control. The lowest PI is obtained via OSOF control.

It may be noted that the solution of Equations (23), (25), and (26) generally yields multiple local minima of the performance index J. Convergence to a particular minima is greatly influenced by the choice of initial stabilizing gain ($\mathbf{K}_0$). The present (Moerder and Calise) algorithm used to solve the OSOF problem does not yield the global minimum J. Future work would attempt to address this problem (e.g. using homotopy methods). However, as shown in the results, the present algorithm for OSOF control is quite effective.

DOI: 10.1002/stc

REFERENCES

1. Housner GW, Bergman LA, Caughey TK, Chassiakos AG, Claus RO, Masri SF, Skelton RE, Soong TT, Spencer BF, Yao JTP. Structural control: past, present, and future. *Journal of Engineering Mechanics* (ASCE) 1997; **123**(9):897–971.
2. Yang G, Spencer Jr BF, Carlson JD, Sain MK. Large-scale MR fluid dampers: modelling and dynamic performance considerations. *Engineering Structures* 2002; **24**:309–323.
3. Ehrgott RC, Masri SF. Modeling the oscillatory dynamic behavior of electrorheological materials in shear. *Smart Materials and Structures* 1992; **1**:275–285.
4. Song X, Ahmadian M, Southward SC. Modeling magnetorhelogical dampers with application of nonparametric approach. *Journal of Intelligent Material Systems and Structures* 2005; **16**:421–432.
5. Stanway R, Sproston JL, Stevens NG. Nonlinear modelling of an electrorhelogical vibration damper. *Journal of Electrostatics* 1987; **20**:167–184.
6. Wen YK. Method for random vibration of hysteretic systems. *Journal of Engineering Mechanics Division* (ASCE) 1976; **102**:249–263.
7. Wong CW, Ni YQ, Ko JM. Steady state oscillation of hysteretic differential model II: performance analysis. *Journal of Engineering Mechanics* (ASCE) 1994; **120**(11):2299–2325.
8. Spencer Jr BF, Dyke SJ, Sain MK, Carlson JD. Phenomenological model of a magnetorhelogical damper. *Journal of Engineering Mechanics* (ASCE) 1996; **123**(3):230–238.
9. Dominguez A, Sedaghati R, Stiharu I. A new dynamic hysteresis model for magnetorhelogical dampers. *Smart Materials and Structures* 2006; **15**:1179–1189.
10. Wang LX, Kamath H. Modelling hysteretic behaviour in magnetorhelogical fluids and dampers using phase-transition theory. *Smart Materials and Structures* 2006; **15**:1725–1733.
11. Jiménez R, Álvarez-Icaza L. LuGre friction model for a magnetorhelogical damper. *Structural Control and Health Monitoring* 2005; **12**:91–116.
12. Canudas de Wit C, Olsson H, Åström KJ, Lischinsky P. A new model for control of systems with friction. *IEEE Transactions on Automatic Control* 1995; **40**(3):419–425.
13. Sakai C, Ohmori H, Sano A. Modeling of MR damper with hysteresis for adaptive vibration control. *Proceedings of the 42nd IEEE Conference on Decision and Control*, Maui, Hawaii, U.S.A., December 2003.
14. Yao GZ, Yap FF, Chen H, Li WH, Yeo SH. MR damper and its application for semi-active control of vehicle suspension system. *Mechatronics* 2002; **12**:963–973.
15. Xu ZD, Shen YP. Intelligent bi-state control for the structure with magnetorhelogical dampers. *Journal of Intelligent Material Systems and Structures* 2003; **14**:35–42.
16. Dyke SJ, Spencer Jr BF, Sain MK, Carlson JD. Seismic response reduction using magnetorhelogical dampers. *Proceedings of the IFAC World Congress*, San Franscisco, CA, 30 June–5 July 1996.
17. Jansen LM, Dyke SJ. Semi-active control strategies for MR dampers: a comparative study. *Journal of Engineering Mechanics* 2000; **126**(8):795–803.
18. Chang CC, Zhou L. Neural network emulation of inverse dynamics for a magnetorhelogical damper. *Journal of Structural Engineering* (ASCE) 2002; **128**(2):231–239.
19. Yuen KV, Shi Y, Beck JL, Lam HF. Structural protection using MR dampers with clipped robust reliability-based control. *Structural Multidisciplinary Optimization* 2007; **34**:431–443.
20. Yoshida O, Dyke SJ. Seismic control of a nonlinear benchmark building using smart dampers. *Journal of Engineering Mechanics* (ASCE) 2004; **134**(4):386–392.
21. Spencer Jr BF. *Reliability of Randomly Excited Hysteretic Structures*. Springer: New York, 1986.
22. Vibration Data El Centro Earthquake Page. Available from: http://www.vibrationdata.com/elcentro.htm [24 December 2008].
23. Lewis FL, Syrmos VL. Optimal Control. Wiley: New York, U.S.A., 1995; 359–370.
24. Chu SY, Soong TT, Reinhorn AM. *Active, Hybrid and Semi-active Structural Control—A Design and Implementation Handbook*. Wiley: England, U.K., 2005; 183–184.
25. Levine WS, Michael A. The determination of the optimal constant output feedback gains for linear multivariable systems. *IEEE Transactions on Automatic Control* 1970; **AC-15**:44–48.
26. Moerder DD, Calise AJ. Convergence of a numerical algorithm for calculating optimal output feedback gains. *IEEE Transaction on Automatic Control* 1985; **AC-30**(9):900–903.
27. Dyke SJ. Acceleration feedback control strategies for active and semi-active control systems: modeling, algorithm development, and experimental verification. *Ph.D. Thesis*, Department of Civil Engineering and Geological Sciences, Notre Dame, IN, U.S.A., July 1996.

DOI: 10.1002/stc